Direct and selective elimination of specific prions and amyloids by 4,5-dianilinophthalimide and analogs

Huan Wang*, Martin L. Duennwald†, Blake E. Roberts*, Leslie M. Rozeboom‡, Yingxin L. Zhang‡, Andrew D. Steele†‡, Rajaraman Krishnan†, Linhui Julie Su†, Drees Griffin†, Samrat Mukhopadhyay§, Edward J. Hennessy¶, Peter Weigele‡, Barbara J. Blanchard‡, Jonathan King‡, Ashok A. Deniz§, Stephen L. Buchwald¶, Vernon M. Ingram‡‖, Susan Lindquist†‡**, and James Shorter*,**

*Department of Biochemistry and Biophysics, University of Pennsylvania School of Medicine, 805b Stellar–Chance Laboratories, 422 Curie Boulevard, Philadelphia, PA 19104; †Whitehead Institute for Biomedical Research, 9 Cambridge Center, Cambridge, MA 02142; Departments of ‡Biology and ¶Chemistry, Massachusetts Institute of Technology, Cambridge, MA 02139; and §Department of Molecular Biology, The Scripps Research Institute, La Jolla, CA 92037

Contributed by Susan Lindquist, March 6, 2008 (sent for review February 4, 2008)

Mechanisms to safely eliminate amyloids and preamyloid oligomers associated with many devastating diseases are urgently needed. Biophysical principles dictate that small molecules are unlikely to perturb large intermolecular protein–protein interfaces, let alone extraordinarily stable amyloid interfaces. Yet 4,5-dianilinophthalimide (DAPH-1) reverses Aβ42 amyloidogenesis and neurotoxicity, which is associated with Alzheimer's disease. Here, we show that DAPH-1 and select derivatives are ineffective against several amyloidogenic proteins, including tau, α-synuclein, Ure2, and PrP, but antagonize the yeast prion protein, Sup35, *in vitro* and *in vivo*. This allowed us to exploit several powerful new tools created for studying the conformational transitions of Sup35 and decipher the mechanisms by which DAPH-1 and related compounds antagonize the prion state. During fibrillization, inhibitory DAPHs alter the folding of Sup35's amyloidogenic core, preventing amyloidogenic oligomerization and specific recognition events that nucleate prion assembly. Select DAPHs also are capable of attacking preformed amyloids. They remodel Sup35 prion-specific intermolecular interfaces to create morphologically altered aggregates with diminished infectivity and self-templating activity. Our studies provide mechanistic insights and reinvigorate hopes for small-molecule therapies that specifically disrupt intermolecular amyloid contacts.

There are no effective treatments for any of the cardiovascular, systemic, or neurodegenerative amyloidoses, including Alzheimer's disease (AD), that afflict humans (1). These stem from specific aberrations in protein folding, which produce a surprisingly generic fibrous conformation termed amyloid. Although amyloid is tightly linked with disease, in many cases, preamyloid oligomers may be the more toxic species (1). Once initiated, amyloidogenesis rapidly amplifies because amyloid fibers self-template their specific conformation at their ends by converting other copies of the same polypeptide to the amyloid form (2). Prions are specialized amyloids that efficiently disseminate and transmit this self-templating activity between cells and even organisms (3). Prions transmit lethal neurodegenerative disorders like variant Creutzfeldt–Jakob disease in humans (3).

Chemical space may harbor small molecules that antagonize the protein–protein interactions that maintain amyloid fibers and preamyloid oligomers. Yet no small-molecule drugs that disrupt protein–protein interactions are approved (4). Dogma holds that it is inherently difficult for small molecules of limited steric bulk to disrupt protein–protein interfaces because of their large, flat surface area (750–1,500 Å^2), which seems to offer limited opportunities for small-molecule insertion (4). For amyloids, this issue is accentuated by their extremely stable intermolecular contacts, which generally require high denaturant concentrations to disrupt (2). Nevertheless, several promising candidates exist for both globular (4) and amyloidogenic proteins (5–8). For globular proteins, crystal structures reveal that small molecules act directly, through the plasticity of the interface, or allosterically, by inducing conformational change at distant sites (4). If the soluble native structure of an amyloidogenic protein is known, as for transthyretin, small molecules that stabilize this form preclude amyloidogenesis (9). Unfortunately, amyloidogenic proteins are often natively unfolded in their soluble states (2). Here, small molecules may divert proteins down alternative aggregation trajectories or trap preamyloid conformers (5–8). However, their mechanism of action is unclear.

Amyloid forms of proteins adopt a cross-β structure in which the β-sheet strands run orthogonal to the fiber axis (2). Preamyloid oligomers possess structural features, distinct from fibers, that are recognized by conformation-specific antibodies and shared by many amyloidogenic proteins (10). Although local steric details may vary enormously (2, 11), these similarities suggest that agents that antagonize amyloid fibers or oligomers of one protein may be active against those formed by another. Indeed, some small molecules, including Congo Red (CR) and (−)-epigallocatechin-3-gallate inhibit amyloidogenesis of several proteins (6–8). Broad specificity, however, may be undesirable because amyloids and prions also can be adaptive (3). For example, the yeast prion, [*PSI*$^+$], comprises Sup35 amyloids and confers phenotypic diversity and selective advantages (3). Further, Pmel17 amyloids mediate melanosome biogenesis, and CPEB prions might act in long-term potentiation (3). Ideally, small molecules would specifically target pathogenic but not beneficial amyloids. Indeed, some small molecules are specific toward particular amyloidogenic proteins (7), but the basis of this is unclear. Understanding this specificity may facilitate the next generation of small molecules that target specific amyloids.

We sought small molecules with selectivity against Aβ42 fibers, a histopathological hallmark of AD (1), which also might be active against Sup35. There are two reasons for choosing Sup35. First, although Sup35 and Aβ42 possess no sequence similarity, they convert to amyloid by a similar process (10, 12–15). Second, Sup35 is one of the best-studied amyloidogenic proteins. A series of fluorescence tools that exist to probe Sup35 amyloidogenesis are not yet available for other amyloids and offer the prospect of

Author contributions: H.W., M.L.D., B.E.R., L.M.R., Y.L.Z., A.D.S., R.K., L.J.S., D.G., S.M., E.J.H., B.J.B., A.A.D., S.L.B., V.M.I., S.L., and J.S. designed research; H.W., M.L.D., B.E.R., L.M.R., Y.L.Z., A.D.S., R.K., L.J.S., D.G., S.M., E.J.H., P.W., B.J.B., and J.S. performed research; E.J.H. and S.L.B. contributed new reagents/analytic tools; H.W., M.L.D., B.E.R., L.M.R., Y.L.Z., A.D.S., R.K., L.J.S., D.G., S.M., B.J.B., J.K., A.A.D., S.L.B., V.M.I., S.L., and J.S. analyzed data; and M.L.D., S.L., and J.S. wrote the paper.

The authors declare no conflict of interest.

‖Deceased August 17, 2006.

**To whom correspondence may be addressed. E-mail: jshorter@mail.med.upenn.edu or lindquist_admin@wi.mit.edu.

This article contains supporting information online at www.pnas.org/cgi/content/full/0801934105/DCSupplemental.

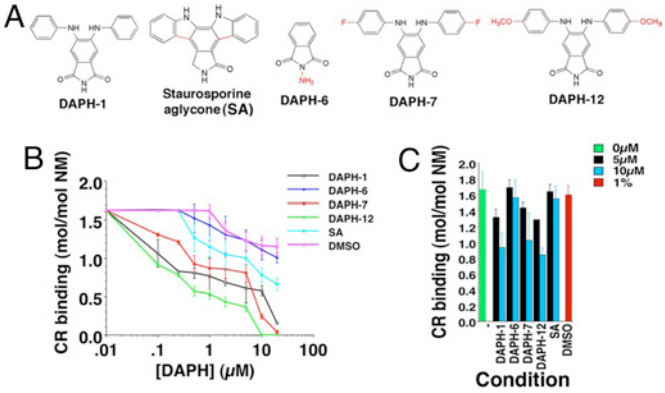

Fig. 1. DAPH-1 and certain analogs inhibit spontaneous and seeded NM fibrillization. (*A*) Chemical structures of DAPH-1 and analogs. Red coloration indicates portions of each analog that differ from the DAPH-1 structure. (*B*) Spontaneous, rotated (80 rpm) NM (5 μM) fibrillization after 4 h in the presence of either DAPH-1, DAPH-6, DAPH-7, DAPH-12, SA (0–20 μM), or DMSO (0–2%). Fibrillization was monitored by CR binding. Values represent means ± SD (n = 6). (*C*) Seeded (2% wt/wt) NM (5 μM) fibrillization after 2 h in the absence or presence of either DAPH-1, DAPH-6, DAPH-7, DAPH-12, SA (5–10 μM), or DMSO (1%). Fibrillization was monitored by CR binding. Values are means ± SD (n = 3).

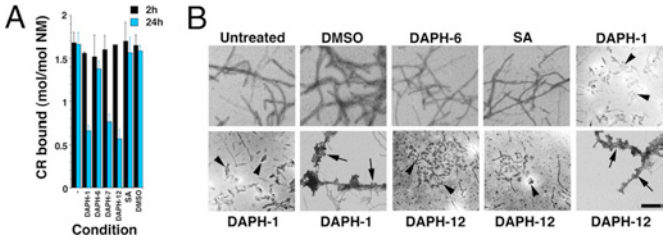

Fig. 2. DAPH-1 and certain analogs remodel NM fibers. (*A*) NM fibers (2.5 μM monomer) were incubated without or with the indicated DAPH (20 μM) or DMSO (2%) for 2 or 24 h at 25°C. Fiber integrity was measured by CR binding. Values are means ± SD (n = 6–14). (*B*) NM fibers (2.5 μM monomer) were incubated with or without the indicated DAPH (20 μM), SA (20 μM), or DMSO (2%) for 24 h at 25°C and processed for EM. (Scale bar: 0.2 μm.) Arrows denote globular masses. Arrowheads denote oligomers or protofibrils.

attaining new mechanistic insight into how small molecules affect amyloid assembly and disassembly (16, 17).

Sup35 is a translation termination factor. Sup35's N-terminal (N) and highly charged middle (M) domains allow switching between the soluble nonprion conformation of [*psi*$^-$] cells and the prion conformation of [*PSI*$^+$] cells in a stable, heritable manner (18, 19). M is highly charged; it confers Sup35 solubility *in vitro* (20) and promotes the [*psi*$^-$] state *in vivo* (18). N confers amyloidogenicity *in vitro* (20) and drives Sup35 prionogenesis *in vivo* (19). *In vitro*, NM fibrillization occurs after a lag phase (13, 20). At low protein concentrations where NM does not assemble, NM monomers rapidly collapse to a premolten globule-like, natively unfolded form that samples with great rapidity multiple transient conformations (13, 17). This might include the prion conformation, but stabilization of that conformation requires protein–protein contacts that occur in similarly molten oligomers that form at higher protein concentrations (13, 14). These oligomers gradually morph into a more structured, amyloidogenic species that nucleates conversion and conformational replication (3, 13–15). Short prion recognition elements within N, termed the "Head" (residues ≈25–38) and "Tail" (residues ≈91–106), make homotypic intermolecular contacts such that fibers are constructed by alternating Head-to-Head and Tail-to-Tail interfaces (16). The Head establishes productive interactions first, which nucleate amyloidogenesis (16, 21). The Tail can also nucleate assembly, but with slower kinetics (21). Sup35 fibers formed *in vitro* transform [*psi*$^-$] cells to the [*PSI*$^+$] state (15).

4,5-Dianilinophthalimide (DAPH-1) inhibits and reverses the formation of Aβ42 fibers and reduces their toxicity to neurons in culture (5). This finding is surprising because DAPH-1 is a tyrosine kinase inhibitor with specificity for the EGF receptor (22). Here, we show how DAPH-1 and analogs selectively affect Sup35 and Aβ42 fibrillization. We employ DAPHs as mechanistic probes to understand how Sup35 transitions to and from the prion state. Our studies reveal how small molecules can affect the folding landscapes of amyloid assembly and disassembly.

Results

DAPH-1 and Certain Analogs Inhibit Spontaneous NM Fibrillization. At low micromolar concentrations, DAPH-1 (Fig. 1*A*) inhibits Aβ42 fibrillization (5). DAPH-1 also inhibited the fibrillization of NM, Sup35's prion-determining region, at concentrations that were 50-fold lower than the concentration of monomeric NM (Fig. 1*B*). The IC_{50} was ≈0.58 μM, and little assembly occurred when DAPH-1 was at a 4-fold molar excess over NM (Fig. 1*B*). DMSO, the DAPH solvent, had very little effect on NM fibrillization (Fig. 1*B*). Similar results were obtained by using other measures of amyloidogenesis, including Thioflavin-T (ThT) fluorescence, sedimentation analysis, and SDS resistance [supporting information (SI) Fig. S1 *A–C*].

We sought to potentiate this activity and tested several DAPH analogs. Staurosporine aglycone (SA), which is structurally similar to DAPH-1 but contains two extra carbon–carbon bonds (Fig. 1*A*) that impose planarity (Fig. S1*D*), was much less effective in inhibiting NM fibrillization (Fig. 1*B*). Similarly, a derivatized phthalimide fragment, DAPH-6 (Fig. 1*A*), did not inhibit NM fibrillization (Fig. 1*B*). However, two DAPH analogs, DAPH-7 and DAPH-12 (Fig. 1*A*), bearing modifications to the aniline rings at position 4 strongly inhibited NM fibrillization (Fig. 1*B*). The IC_{50} was ≈3.4 μM for DAPH-7, but DAPH-12 had an IC_{50} of ≈0.18 μM and was more potent than DAPH-1. DAPH-12 does not inhibit tyrosine kinases (22). Thus, the ability of DAPH to inhibit amyloidogenesis is separated from the inhibition of tyrosine kinases.

We tested whether DAPHs also could inhibit the fibrillization of tau, α-synuclein, and Ure2. In contrast to their effects on Aβ42 and NM, DAPH-1 and DAPH-7 did not inhibit amyloidogensis of tau, α-synuclein, or Ure2 (*SI Results* and Fig. S2*A*). Thus, DAPH-1 selectively inhibits amyloidogenesis of Aβ42 and NM despite their lack of primary sequence similarity.

DAPH-1 and Certain Analogs Inhibit Seeded NM Fibrillization. Could DAPHs interfere with assembly seeded by NM fibers? Intriguingly, DAPHs were less effective in inhibiting seeded assembly as assessed by CR binding (Fig. 1*C*) and SDS resistance (data not shown). Indeed, concentrations of DAPH-12 that eliminated spontaneous NM assembly failed to inhibit seeded assembly by 50% (Fig. 1*C*). DAPH-6 and SA were ineffective. These data establish that DAPHs do not inhibit CR binding by some nonspecific mechanism. Moreover, DAPH-1 and analogs are most active before the formation of the intermolecular contacts that drive NM fibrillization.

DAPH-1 and Certain Analogs Remodel NM Fibers. At low micromolar concentrations, DAPH-1 partially dissolves Aβ42 fibers (5). Can DAPHs also act directly on NM fibers? After 2 h in the presence of a 4-fold molar excess of small molecule, little change in NM fiber integrity occurred as monitored by CR or ThT binding (Fig. 2*A*) (data not shown), again demonstrating that DAPHs do not interfere with these assays by some nonspecific mechanism. After 24 h, DAPH-6 and SA had little effect on NM fibers (Fig. 2*A*). However, DAPH-1, DAPH-7, and DAPH-12 reduced CR or ThT binding by >45% (Fig. 2*A*) (data not shown) after 24 h. Importantly, DAPH-1 and DAPH-7 did not affect tau, α-syn, or

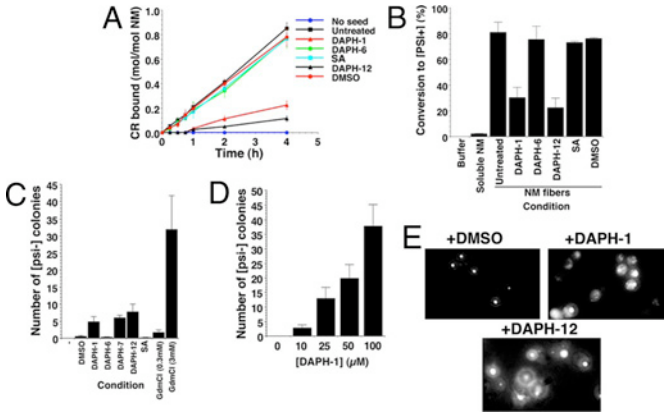

Fig. 3. DAPH-1 and certain analogs eradicate prions *in vitro* and *in vivo*. (*A* and *B*) NM fibers (2.5 μM monomer) were treated with either DAPH-1, DAPH-6, DAPH-12, SA (20 μM), or DMSO (2%) for 24 h at 25°C. (*A*) Reaction products were collected by ultracentrifugation, washed with buffer, and used to seed (0.5% wt/wt) undisturbed NM (2.5 μM) fibrillization. Values are means± SD ($n = 3$). (*B*) Alternatively, products were transformed into [*psi*$^-$] cells. The number of [*PSI*$^+$] colonies relative to total transformants was determined. Values are means ± SD ($n = 3$). (*C*) [*PSI*$^+$] Δ*PDR5* yeast cells were treated with either DMSO (1%), DAPH-1 (50 μM), DAPH-7 (50 μM), DAPH-12 (50 μM), or GdmCl (0.3 mM or 3 mM) for 15 h in liquid culture. Cells were plated on YPD, and the number of red [*psi*$^-$] colonies was determined. Values are means ± SD ($n = 3$). (*D*) [*PSI*$^+$] Δ*PDR5* yeast cells were treated with DAPH-1 (0–100 μM) for 24 h in liquid culture. Cells were plated on 25% YPD, and the number of red [*psi*$^-$] colonies was determined. Values are means ± SD ($n = 3$). (*E*) NM-YFP was expressed for 4 h in [*PSI*$^+$] Δ*PDR5* yeast cells. Expression was then shut down in the presence of DMSO (1%), DAPH-1, or DAPH-12 (200 μM) for 2 h, and cells were then imaged. Note the more diffuse NM-YFP staining of DAPH-1- and DAPH-12-treated cells.

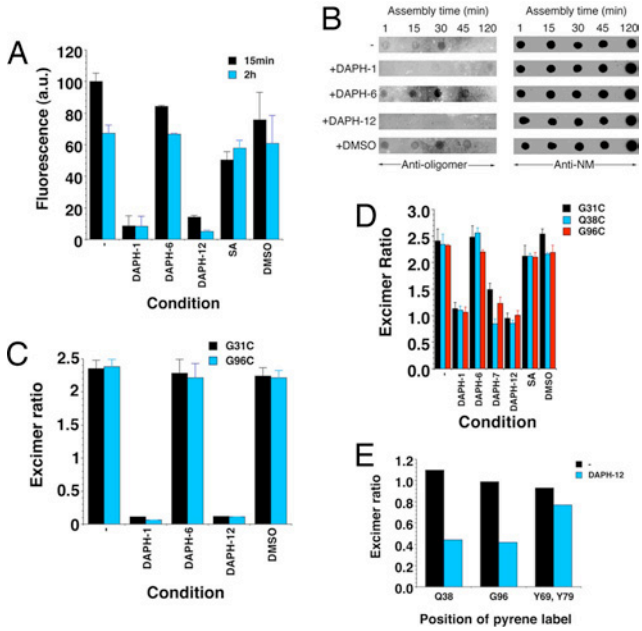

Fig. 4. DAPH-1 and DAPH-12 interfere with early events in NM fibrillization and break intermolecular contacts of NM fibers. (*A*) Fluorescence of NM G96C-acrylodan (5 μM) after 15 min (black bars) or 2 h (blue bars) of rotation (80 rpm) in the absence or presence of either DAPH-1, DAPH-6, DAPH-12, SA (10 μM), or DMSO (1%). Values are means ± SD ($n = 3$). (*B*) Spontaneous, rotated (80 rpm) NM (5 μM) fibrillization in the absence or presence of DAPH-1, DAPH-6, or DAPH-12 (10 μM) or DMSO (1%). At various times, reactions were applied to nitrocellulose and probed with anti-oligomer antibody or anti-NM antibody. (*C*) Excimer fluorescence of NM G31C-pyrene (black) or G96C-pyrene (blue) (5 μM) after 2h spontaneous, rotated (80 rpm) assembly in the absence or presence of DAPH-1, DAPH-6, DAPH-12 (10 μM), or DMSO (1%). The ratio of excimer fluorescence to nonexcimer fluorescence ($I_{465\ nm}/I_{375\ nm}$) is plotted. Values are means ± SD ($n = 3$). (*D*) NM fibers (2.5 μM monomer) labeled with pyrene at G31C (black bars), Q38C (blue bars), or G96C (red bars) were incubated in the absence or presence of the indicated DAPH (20 μM), SA (20 μM), or DMSO (2%) for 24 h at 25°C. The ratio of excimer fluorescence to nonexcimer fluorescence ($I_{465\ nm}/I_{375\ nm}$) is plotted. Values are means ± SD ($n = 3$). (*E*) NM fibers (2.5 μM monomer) labeled with pyrene at Q38C, G96C, or Y69C plus Y79C were incubated in the absence or presence of DAPH-12 (20 μM) for 24 h at 25°C. The ratio of excimer fluorescence to nonexcimer fluorescence ($I_{465\ nm}/I_{375\ nm}$ for Q38 and G96, and $I_{476\ nm}/I_{384\ nm}$ for Y69C plus Y79C) is plotted.

Ure2 fibers (*SI Results* and Fig. S2*B*), nor did they affect mammalian prions (*SI Results* and Fig. S2*C*). Thus, DAPH-1 targets a feature of NM and Aβ42 fibers that is not shared by tau, α-syn, and Ure2.

Next, we examined the effects of DAPHs by EM. Treatment of NM fibers for 2 h with DAPH-1 or DAPH-12, or 24 h with DAPH-6, SA, or DMSO had little effect on fiber morphology (Fig. 2*B*) (data not shown). By contrast, 24-h treatments with DAPH-1 or DAPH-12 converted fibers to collections of small fragments with elliptical or tubular profiles, perhaps indicative of oligomers and protofibrils (Fig. 2*B*, arrowheads). Such profiles were not seen in control samples containing only DAPHs (data not shown). In rare fields, fibers persisted, but had a more ragged appearance or were converted to globular masses (Fig. 2*B*, arrows). Thus, DAPH-1 and DAPH-12 convert NM fibers to several distinct aggregated forms.

DAPH-1 and DAPH-12 Diminish the Self-Replicating, Infectious Nature of NM Fibers. How do DAPH treatments of NM fibers affect their prion nature? To test this question, we treated fibers with various DAPHs for 2 or 24 h, collected the reaction products by ultracentrifugation, and washed extensively with buffer to remove any remaining small molecule (*SI Materials and Methods*). Approximately equal amounts of NM were recovered from each condition (*SI Materials and Methods*). We then tested their ability to seed assembly of soluble NM and to transform [*psi*$^-$] cells to [*PSI*$^+$]. Treatment of NM fibers for 2 h with DAPHs, SA, or DMSO had no effect on seeding or [*PSI*$^+$]-inducing activity (data not shown). Even after 24 h, DAPH-6, SA, or DMSO had no effect on seeding activity or [*PSI*$^+$]-inducing activity (Fig. 3 *A* and *B*). By contrast, after 24 h, DAPH-1 and DAPH-12 reduced both seeding activity *in vitro* and the amount of [*PSI*$^+$] induction (Fig. 3 *A* and *B*). Thus, remodeling of NM fibers by DAPH-1 and DAPH-12 reduces both their self-replicating activity and infectious nature.

DAPH-1 and Certain Analogs Cure [*PSI*$^+$]. Small molecules that are active *in vitro* are often inactive *in vivo* because they fail to enter cells; have unexpected, nonspecific interactions with other targets; or are metabolized into inactive forms. To test whether DAPHs target specific amyloids *in vivo*, we examined their [*PSI*$^+$]-curing ability. We used a strain lacking the ABC transporter, Pdr5, which pumps small molecules out of the cell. Δ*PDR5* cells stably propagated [*PSI*$^+$] (Fig. 4*C*). DMSO (>5%) cures [*PSI*$^+$], and some [*psi*$^-$] colonies appeared with 1% DMSO (Fig. 3*C*). DAPH-6 and SA caused no further increase in the appearance of [*psi*$^-$] colonies (Fig. 3*C*). By contrast, DAPH-1, DAPH-7, and DAPH-12 cured [*PSI*$^+$] more effectively: ≈5- to 7-fold more [*psi*$^-$] colonies appeared than with DMSO (Fig. 3*C*). DAPH-1 mediated curing was dose-dependent (Fig. 3*D*). Importantly, DAPHs did not cure [*RNQ*$^+$] prions (3, data not shown). Thus, DAPH-1, DAPH-7, and DAPH-12 retain selectivity *in vivo* and are specific [*PSI*$^+$]-curing agents.

We compared DAPH efficacy to a well established [*PSI*$^+$]-curing agent, GdmCl (3). GdmCl cures [*PSI*$^+$], [*URE3*], and [*RNQ*$^+$] by

BIOCHEMISTRY

inhibiting the prion-fragmenting activity of Hsp104 (3, 15). That DAPH-1, DAPH-7, and DAPH-12 specifically cure [*PSI*$^+$] and not [*RNQ*$^+$] indicates that they do not inhibit Hsp104. Indeed, Hsp104 ATPase activity was unaffected by a 10-fold molar excess of DAPH-1 or DAPH-12 (data not shown). GdmCl (3 mM) was more effective than the DAPH-1, DAPH-7, and DAPH-12 in [*PSI*$^+$] curing, although lower concentrations (0.3 mM) were less effective (Fig. 3*C*).

Do DAPHs alter Sup35 prion aggregation *in vivo*? To test this idea, we used NM-YFP, which forms fluorescent foci in [*PSI*$^+$] cells, but is diffuse in [*psi*$^-$] cells (19). [*PSI*$^+$] cells treated with DMSO all contain one discrete, tight fluorescent focus (Fig. 3*E*), which is indicative of [*PSI*$^+$]. However, DAPH-1 or DAPH-12 increased diffuse cytoplasmic NM-YFP fluorescence (Fig. 3*E*). Furthermore, ≈30% of cells lacked foci altogether or contained diffuse fluorescence plus NM-YFP fluorescent foci with a distinct fragmented or less tightly organized morphology (Fig. 3*E*). This finding suggests that DAPH-1 and DAPH-12 promote prion curing by altering Sup35 aggregation. Thus, DAPHs are potent and selective amyloid-remodeling agents *in vitro* and *in vivo*.

DAPH-1 and DAPH-12 Disrupt the Earliest Events in NM Fibrillization. Several steps during lag phase could be attenuated by inhibitory DAPHs. First, an equilibrium forms between premolten globule-like, natively unfolded NM monomers and molten oligomers (13). Single-cysteine NM mutants labeled with acrylodan can be used to track these events (16). Acrylodan is extremely sensitive to its immediate environment, and changes in fluorescent intensity and emission maximum occur upon reductions in the local environmental dielectric constant. Studies with acrylodan-labeled NM indicate residues 21–106 of N are rapidly shielded from solvent (16). However, it is unclear whether this result is due to oligomerization or monomer compression detected by single-molecule FRET (17). We used DAPHs to probe the importance of these events for NM fibrillization.

We tested how DAPHs affect the early events of lag phase by employing NM G96C-acrylodan. This label alters neither NM assembly kinetics (16) nor the final prion state because NM G96C-acrylodan fibers have the same infectivity as NM fibers (R.K. and S.L., unpublished data). NM G96C-acrylodan fluorescence increased rapidly during early lag phase and was complete after 15 min, which preceded the end of lag phase by ≈15 min (16). This was unaffected by DMSO or DAPH-6 (Fig. 4*A*), conditions that do not affect NM fibrillization (Fig. 1*B*). SA, which inhibits assembly by ≈50% (Fig. 1*B*), reduced the fluorescence increase by ≈50% (Fig. 4*A*). DAPH-1 and DAPH-12 blocked this rapid fluorescence increase (Fig. 4*A*). Even after 2 h, acrylodan fluorescence remained low in the presence of DAPH-1 or DAPH-12 (Fig. 4*A*). Very similar data were obtained by using NM N21C-acrylodan (data not shown). Thus, the collapsed state revealed by increased acrylodan fluorescence is essential for NM fibrillization and is abrogated by DAPH-1 and DAPH-12, which render the amyloid-core region (amino acids 21–106) more solvent-accessible.

Unfortunately, acrylodan fluorescence does not distinguish between NM monomers and oligomers. Thus, we used single-molecule FRET (17) to test whether DAPH-1 affects the compression of NM monomers that occurs early in lag phase. Intriguingly, 0.1 μM DAPH-1 had no effect on the single-molecule FRET peak for 100 pM NM labeled with Alexa Fluor 488 at position 21 and Alexa Fluor 594 at position 121 (Fig. S3*A*). DAPH-1 also had no effect on the fast conformational fluctuations of NM monomers (labeled with Alexa488 at position 38) revealed by fluorescence correlation spectroscopy (Fig. S3*B*) (17). Thus, DAPH-1 does not affect NM monomer compression or conformational dynamics, but rather affects NM oligomers, which harbor the critical intermediates for prion nucleation (13, 14).

DAPH-1 and DAPH-12 Inhibit the Maturation of Molten NM Oligomers. DAPH-1 and DAPH-12 might reduce the proportion of NM that forms molten oligomers, which can retard fibrillization (13). However, the amount of NM retained by a 50-kDa filter at the beginning of lag phase (14) remained constant at ≈10% of total NM in the presence or absence of DAPH-1, DAPH-6, DAPH-12, 10 μM SA, or 1% DMSO. Thus, the proportion of NM that forms molten oligomers was unaffected. Further, fluorescence polarization anisotropy of NM labeled (at either position 38, 51, 77, or 96) with IAEDANS demonstrated that DAPH-1 had no effect on molten oligomer formation (data not shown).

Do DAPHs inhibit the maturation of molten NM oligomers to an amyloidogenic conformation, which nucleates fibrillization? To detect this obligate reaction intermediate, we used a conformation-specific antibody that recognizes mature NM oligomers, but not NM fibers or monomers (14). At select times during NM fibrillization, aliquots were applied to nitrocellulose and probed with antibodies (14). An anti-NM antibody recognized NM at all stages (Fig. 4*B*). By contrast, anti-oligomer immunoreactivity peaked at the end of lag phase (30 min) and then rapidly disappeared (Fig. 4*B*). DMSO or DAPH-6, which had little effect on fibrillization, had little effect on amyloidogenic oligomer formation (Fig. 4*B*). Remarkably, DAPH-1 and DAPH-12 inhibited amyloidogenic oligomer formation (Fig. 4*B*). Thus, DAPH-1 and DAPH-12 prevent the rearrangements of NM molecules within molten oligomers that are required to generate amyloidogenic oligomers that nucleate fibrillization.

DAPH-1 and DAPH-12 Inhibit *de Novo* Nucleating Intermolecular Contacts. DAPH-1 and DAPH-12 may prevent either Head-to-Head or Tail-to-Tail contact formation or both to arrest fibrillization. Hence, we used NM single-cysteine mutants labeled with pyrene in either the head (G31C) or the tail (G96C) region. Upon intermolecular contact formation and fibrillization, pyrene molecules form excimers (excited-state dimers) that produce a strong red shift in fluorescence. Neither DMSO nor DAPH-6 had any effect on intermolecular contact formation (Fig. 4*C*). However, DAPH-1 and DAPH-12 blocked both spontaneous Head-to-Head and Tail-to-Tail contact formation (Fig. 4*C*). Thus, DAPH-1 and DAPH-12 inhibit prion nucleation by preventing both Head-to-Head and Tail-to-Tail intermolecular interactions.

DAPH-1 and DAPH-12 Break Prion-Specific Intermolecular Contacts in NM Fibers. Can DAPHs break the intermolecular contacts of NM fibers? To test this question, we assembled fibers of NM G31C-pyrene, Q38C-pyrene (to assess Head-to-Head contacts), or G96C-pyrene (to assess Tail-to-Tail contacts) and then treated with various DAPHs. DAPH-6, SA, and DMSO had little effect on the integrity of Head-to-Head or Tail-to-Tail contacts (Fig. 4*D*), which is consistent with their lack of effects on CR binding (Fig. 2*A*) or NM fiber integrity (Fig. 2*B*). DAPH-1, DAPH-7, and DAPH-12 reduced excimer fluorescence by ≈40–65% at G31, Q38, or G96 (Fig. 4*D*). DAPH-1 and DAPH-12 were the most potent. These data suggest that DAPH-1 and DAPH-12 break Head-to-Head and Tail-to-Tail contacts.

Were these DAPHs specifically targeting the intermolecular interfaces of NM fibers or indiscriminately disrupting inter- and intramolecular contacts? To test this question, we used a double-cysteine NM mutant (Y69C, Y79C) labeled with pyrene, which forms excimers only in NM fibers because of intramolecular contact between residues 69 and 79 in the fiber core (R.K. and S.L., unpublished data). Remarkably, DAPH-12 only slightly reduced this intramolecular excimer fluorescence, compared with intermolecular excimer fluorescence (Fig. 4*E*). Thus, intramolecular interactions within the fiber core may remain unperturbed. This finding also indicates that DAPH-12 does not interfere with pyrene excimer fluorescence by some nonspecific mechanism. Hence, remodeling of NM fibers by DAPH-1 and DAPH-12 likely involves the

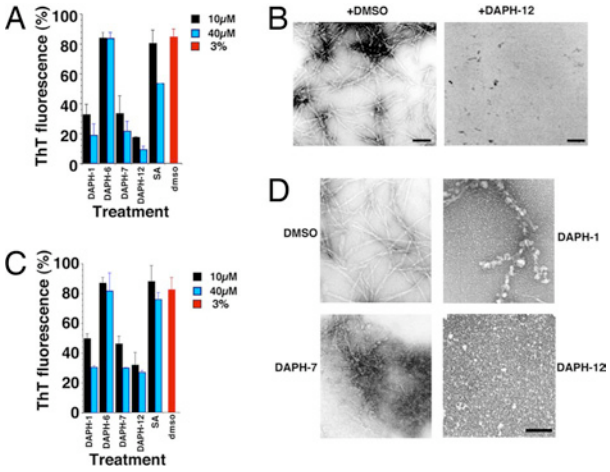

Fig. 5. Inhibition and reversal of Aβ42 fibrillization by DAPH-1, DAPH-7, and DAPH-12. (*A*) Aβ42 (10 μM) was incubated for 24 h with the indicated DAPH, SA (10 or 40 μM), or DMSO (2%). Fibrillization was determined by ThT fluorescence; 100% assembly reflects Aβ42 assembly in the absence of DAPH, SA, or DMSO. Values are means ± SD ($n = 3$). (*B*) Aβ42 (10 μM) was incubated for 24 h at 37°C with either DMSO (0.1%) or DAPH-12 (10 μM) and then viewed by EM. (Scale bars: 0.1 μm.) (*C*) Aβ42 fibers (10 μM monomer) were incubated with the indicated DAPH, SA (10 or 40 μM), or DMSO (2%) for 1 h at 37°C. Fiber integrity was measured by ThT fluorescence. Values are means ± SD ($n = 3$). (*D*) Aβ42 fibers (10 μM monomer) were treated with the indicated DAPH (10 μM) or DMSO (2%) as in *C* and then viewed by EM. (Scale bar: 0.1 μm.)

breakage and/or rearrangement of the intermolecular contacts that hold NM fibers together. Remarkably, these rearrangements produce a distinct ensemble of aggregates that retain particular intramolecular contacts.

DAPH-7 and DAPH-12 Inhibit and Reverse Aβ42 Fibrillization. Next, we tested whether DAPH-7 and DAPH-12 also inhibited Aβ42 fibrillization. As with NM, DAPH-1, DAPH-7, and DAPH-12 inhibited Aβ42 fibrillization, with DAPH-12 being the most potent (Fig. 5*A*). By contrast, DAPH-6 and SA were much less effective (Fig. 5*A*). EM confirmed that fibrillization was indeed inhibited. Fibers were scarce in the presence of DAPH-1 (5) or DAPH-7 (data not shown). In the presence of DAPH-12, only short prefibrillar structures formed after 24 h, whereas fibers were abundant in the DMSO control (Fig. 5*B*).

Finally, we tested whether DAPHs could remodel preformed Aβ42 fibers. DAPH-6 and SA had little effect on Aβ42 fibers (Fig. 5*C*). By contrast, DAPH-1, DAPH-7, and DAPH-12 remodeled Aβ42 fibers (Fig. 5*C*). This occurred within 1 h and was more rapid than for NM fibers (Fig. 5*C*). EM revealed that Aβ42 fibers were now scarce and had been converted to small oligomers and amorphous masses by DAPH-1, DAPH-7, and DAPH-12 (Fig. 5*D*). Thus, select DAPHs remodel Aβ42 fibers as well as inhibit their *de novo* assembly.

Discussion

We dissected the mechanisms by which a family of small molecules interfere with amyloid assembly and promote amyloid disassembly. Select DAPHs strongly antagonize Aβ42 and NM fibrillization and remodel mature fibers. By contrast, DAPHs had little effect on tau, α-syn, and Ure2 amyloidogenesis or on mammalian prions. Importantly, select DAPHs antagonize amyloid *in vivo* and cure [PSI^+], but not [RNQ^+] prions. Such selectivity and activity in the highly concentrated protein milieu of the yeast cytoplasm seems to argue against a nonspecific mode of inhibition involving colloidal micelles of DAPH (4, 23). Indeed, DAPHs inhibit spontaneous NM fibrillization at substoichiometric concentrations where colloidal micelles cannot be detected. Furthermore, even at the highest DAPH concentrations used here, colloidal micelles make only a minor contribution to DAPH activity (J.S., unpublished data).

Rather, we suggest that DAPHs reveal unsuspected commonalities in the assembly pathways and properties of Aβ42 and NM fibers. These commonalities are surprising given that Aβ42 and NM bear no primary sequence similarity. Indeed, they are profoundly different, even in length and composition. The amyloidogenic region of NM, N, is enriched in uncharged polar amino acids (Gln, Asn, and Tyr make up ≈60% of total amino acids), whereas Aβ42 is enriched in hydrophobic residues (Val, Leu, Ile, and Phe make up ≈33% of total amino acids). Thus, inhibitory DAPHs might recognize a conformational element of obligate assembly intermediates that is common to NM and Aβ42, but not the other amyloidogenic proteins tested.

What might this common element be? DAPHs inhibit Aβ42 and NM assembly at substoichiometric concentrations (5, 7), which suggests they might target a rare or transient conformer that nucleates assembly. DAPHs also might block fiber ends and inhibit assembly. However, at the substoichiometric concentrations that block *de novo* assembly, DAPHs did not inhibit NM assembly seeded by preformed fibers, making this mechanism highly unlikely. Previous experiments with acrylodan fluorescence provided a crucial clue. A fraction of NM molecules reorganize to shield their amyloidogenic core (residues 21–121) from solvent, a process that begins immediately and is completed midway through lag phase (16). Whether this reorganization was required for fibrillization was not clear, nor was it clear whether it involved NM oligomers or monomers. Our findings that inhibitory DAPHs block these events establish that they are essential for fibrillization. DAPHs do not, however, block the compression of NM monomers observed by single-molecule FRET (17). Thus, changes in acrylodan fluorescence reflect events that occur in NM oligomers and are antagonized by specific DAPHs. Moreover, these specific DAPHs preclude the appearance of anti-oligomer immunoreactivity and the establishment of intermolecular contacts that spark fibrillization. Thus, DAPHs interfere directly with molten NM oligomers and prevent their evolution to the form that nucleates prions. The minimal number of NM monomers that must be affected by DAPHs for inhibition of assembly remains unclear. However, this number might be restricted to those NM monomers sequestered in molten oligomers, which amounts to ≈10% of the total NM under a wide range of protein concentrations (13, 24).

Nucleation of Aβ42 and NM fibers requires the formation of specific self-complementary intermolecular contacts (16, 21, 25). But what type of contact might DAPHs prevent? Accumulating evidence implicates the stacking and π–π interactions (intermolecular overlapping of *p*-orbitals) of aromatic amino acids, particularly tyrosine and phenylalanine, in geometric and energetic events that promote amyloidogenesis of some proteins (26). Indeed, in one crystal structure of an amyloid fiber, π–π phenylalanine interactions are critical in zipping antiparallel β-sheets together (27). DAPH appears well suited to inhibiting the formation of or even disrupting such interactions. Phe 19 and 20 of Aβ42 play a crucial role in Aβ42 fibrillization (25, 28, 29). Further, aromatic residues are well represented in Sup35's Head and Tail and may be crucial for fibrillization. Intercalation of DAPH into molten oligomers may prevent aromatic interactions that nucleate fibrillization. The amyloidogenic cores of Ure2, tau, and α-syn have a relative paucity of aromatic residues, which could explain the ineffectiveness of DAPHs in inhibiting their assembly.

DAPH-1 and DAPH-12 remodel Aβ42 and NM fibers. Are there structural features of these fibers, beyond the generic cross-β form, that might explain this commonality? A Sup35 peptide (NNQQ) and an Aβ peptide (GGVVIA) assemble into topologically identical amyloid steric zippers (11). In Aβ42, various DAPHs might antagonize the Phe stacking (25), which helps hold fibers together. No structure of NM fibers is available, but NM fibers are composed of alternating intermolecular Head-to-Head and Tail-to-Tail con-

tacts, which separate a central core region (residues ≈39–90) sequestered by intramolecular contacts. By contrast, Aβ42 fibers comprise purely intermolecular contacts, which may explain why they are more rapidly resolved by DAPHs.

The dry interfaces of amyloid steric zippers revealed in crystal structures appear extremely inaccessible (2, 11). However, we find that DAPHs selectively disrupt the intermolecular Head-to-Head and Tail-to-Tail contacts of NM fibers while leaving particular intramolecular contacts intact. Thus, the intermolecular contacts of Sup35 may be packed differently from the central fiber core. Disruption of intermolecular contacts causes gross rearrangements into distinct aggregates, which lack self-templating activity *in vitro* and *in vivo*. It is likely that amyloid fibers are in equilibrium with oligomers with less well defined intermolecular contacts (30). DAPHs may shift this equilibrium dramatically to the oligomeric form. Disruption of Head-to-Head and Tail-to-Tail contacts and the subsequent loss of prion activity reinforce their importance for conformational replication (16, 21). Definition of intermolecular contacts in other amyloids will help elucidate hotspots for potential pharmacological intervention. This is especially important if intermolecular contacts are generally more sensitive to small molecules than intramolecular contacts, as is the case with Sup35 and the DAPHs. With the advent of more structural information concerning fiber contacts, we hope to develop new therapeutic agents that selectively disrupt amyloid interfaces.

Materials and Methods

Small Molecules. See *SI Materials and Methods* for details on small molecules.

Proteins. Aβ42 was obtained from BioSource. NM and NM cysteine mutants were purified and labeled with either pyrene maleimide or acrylodan as in ref. 16.

Fiber Assembly and Disassembly Reactions. Aβ42 (10 μM) fibers were assembled in Tyrode's/2 mM Ca buffer [150 mM NaCl, 3 mM KCl, 10 mM Hepes (pH 7.4), 2 mM $CaCl_2$, 10 mM D-glucose, and 0.02% NaN_3] with or without the indicated DAPH. Reactions were unagitated and incubated at 37°C for 24–48 h. For disassembly, Aβ42 fibers (10 μM monomer) were incubated at 37°C with the indicated DAPH (0–40 μM) for 0–24 h. Fiber assembly or disassembly was determined by ThT fluorescence or EM as in ref. 5.

NM fiber assembly and disassembly were performed in the presence of the indicated DAPH as in refs. 14 and 16. NM (5 μM) fibrillization was in assembly buffer (AB) [40 mM Hepes-KOH (pH 7.4), 150 mM KCl, 20 mM $MgCl_2$, and 1 mM DTT]. Unseeded reactions were rotated (80 rpm) for 4 h at 25°C. Seeded reactions were unrotated. Fiber assembly or disassembly was determined by EM, SDS resistance, sedimentation analysis, CR binding, or ThT fluorescence as in refs. 14 and 16. See *SI Materials and Methods*.

Biophysical Measurements. Acrylodan and pyrene fluorescence studies were performed as in ref. 16, except that samples were diluted 10-fold in AB before measurement to prevent potential spectroscopic interference. Single-molecule FRET and fluorescence correlation spectroscopy studies were performed as in ref. 17. Fluorescence polarization anisotropy was performed by using a PC1 Photon Counting Spectrofluorometer from ISS. Samples were excited at 337 nm, and emissions at 470 nm (8-nm bandwidth) were recorded.

Protein Transformation. NM fiber transformation was performed as in ref. 16. See *SI Materials and Methods* for additional information.

[*PSI*$^+$]-Curing Experiments. [*PSI*$^+$] Δ*PDR5* yeast cells (W303 Mat α leu2–3,112; his3–11, −15; trp1–1; ura3–1; ade1–4; can1–100 Δpdr5::CAN) growing in mid-log phase (OD_{600} = 0.4–0.6) were left untreated or treated with either DMSO (1%), DAPH-1 (50 μM), DAPH-7 (50 μM), DAPH-12 (50 μM), or GdmCl (0.3 mM or 3 mM) for 15 h in liquid culture. Then ≈10^3 cells were plated on YPD, and the fraction of red ade$^-$ [*psi*$^-$] colonies was determined.

For fluorescence experiments, NM-YFP was expressed from a galactose-inducible plasmid for 4 h in [*PSI*$^+$] Δ*PDR5* yeast cells. Expression was the shut down by adding 2% glucose in the presence of DMSO (1%), DAPH-1, or DAPH-12 (200 μM) for 2 h. Cells were imaged by using a Zeiss Axioplan II fluorescence microscope.

ACKNOWLEDGMENTS. Dedicated to Vernon M. Ingram (1924–2006), an inspirational scientist and treasured colleague. We thank A. Topolszki and N. Watson for technical assistance; C. Glabe, J. Weissman, R. Wickner, P. Lansbury, Jr., and G. Raymond for generous provision of reagents; and A. Gitler, A. Neuhaus-Follini, and K. Molnar for insightful comments on the manuscript. This work was supported by a Huntington's Disease Society of America Postdoctoral Fellowship (to M.L.D.); an American Cancer Society Postdoctoral fellowship (to L.J.S.); National Institutes of Health Grants GM066833 (to A.A.D.) and GM58160 (to S.L.B.); an Alzheimer's Association Investigator Initiated Grant (to V.M.I.); a Kurt and Johanna Immerwahr Fund for Alzheimer Research Grant (to V.M.I.); DuPont–MIT Alliance and National Institutes of Health Grant GM25874 (to S.L., an investigator of the Howard Hughes Medical Institute); an American Heart Association scientist development grant; and University of Pennsylvania Alzheimer's Disease Core Center Pilot AG 10124 and Institute on Aging Pilot (J.S.).

1. Skovronsky DM, Lee VM-Y, Trojanowski JQ (2006) Neurodegenerative diseases: New concepts of pathogenesis and their therapeutic implications. *Annu Rev Pathol Mech Dis* 1:151–170.
2. Nelson R, Eisenberg D (2006) Structural models of amyloid-like fibrils. *Adv Protein Chem* 73:235–282.
3. Shorter J, Lindquist S (2005) Prions as adaptive conduits of memory and inheritance. *Nat Rev Genet* 6:435–450.
4. Arkin MR, Wells JA (2004) Small-molecule inhibitors of protein-protein interactions: Progressing towards the dream. *Nat Rev Drug Discovery* 3:301–317.
5. Blanchard BJ, *et al.* (2004) Efficient reversal of Alzheimer's disease fibril formation and elimination of neurotoxicity by a small molecule. *Proc Natl Acad Sci USA* 101:14326–14332.
6. Ehrnhoefer DE, *et al.* (2006) Green tea (-)-epigallocatechin-gallate modulates early events in huntingtin misfolding and reduces toxicity in Huntington's disease models. *Hum Mol Genet* 15:2743–2751.
7. Masuda M, *et al.* (2006) Small molecule inhibitors of α-synuclein filament assembly. *Biochemistry* 45:6085–6094.
8. Sanchez I, Mahlke C, Yuan J (2003) Pivotal role of oligomerization in expanded polyglutamine neurodegenerative disorders. *Nature* 421:373–379.
9. Hammarstrom P, Wiseman RL, Powers ET, Kelly JW (2003) Prevention of transthyretin amyloid disease by changing protein misfolding energetics. *Science* 299:713–716.
10. Kayed R, *et al.* (2003) Common structure of soluble amyloid oligomers implies common mechanism of pathogenesis. *Science* 300:486–489.
11. Sawaya MR, *et al.* (2007) Atomic structures of amyloid cross-beta spines reveal varied steric zippers. *Nature* 447:453–457.
12. Bitan G, *et al.* (2003) Amyloid β-protein (Aβ) assembly: Aβ40 and Aβ42 oligomerize through distinct pathways. *Proc Natl Acad Sci USA* 100:330–335.
13. Serio TR, *et al.* (2000) Nucleated conformational conversion and the replication of conformational information by a prion determinant. *Science* 289:1317–1321.
14. Shorter J, Lindquist S (2004) Hsp104 catalyzes formation and elimination of self-replicating Sup35 prion conformers. *Science* 304:1793–1797.
15. Shorter J, Lindquist S (2006) Destruction or potentiation of different prions catalyzed by similar Hsp104 remodeling activities. *Mol Cell* 23:425–438.
16. Krishnan R, Lindquist SL (2005) Structural insights into a yeast prion illuminate nucleation and strain diversity. *Nature* 435:765–772.
17. Mukhopadhyay S, Krishnan R, Lemke EA, Lindquist S, Deniz AA (2007) A natively unfolded yeast prion monomer adopts an ensemble of collapsed and rapidly fluctuating structures. *Proc Natl Acad Sci USA* 104:2649–2654.
18. Liu JJ, Sondheimer N, Lindquist SL (2002) Changes in the middle region of Sup35 profoundly alter the nature of epigenetic inheritance for the yeast prion [*PSI*$^+$]. *Proc Natl Acad Sci USA* 99(Suppl 4):16446–16453.
19. Patino MM, Liu JJ, Glover JR, Lindquist S (1996) Support for the prion hypothesis for inheritance of a phenotypic trait in yeast. *Science* 273:622–626.
20. Glover JR, *et al.* (1997) Self-seeded fibers formed by Sup35, the protein determinant of [*PSI*$^+$], a heritable prion-like factor of *S. cerevisiae*. *Cell* 89:811–819.
21. Tessier PM, Lindquist S (2007) Prion recognition elements govern nucleation, strain specificity and species barriers. *Nature* 447:556–561.
22. Trinks U, *et al.* (1994) Dianilinophthalimides: Potent and selective, ATP-competitive inhibitors of the EGF-receptor protein tyrosine kinase. *J Med Chem* 37:1015–1027.
23. McGovern SL, Helfand BT, Feng B, Shoichet BK (2003) A specific mechanism of non-specific inhibition. *J Med Chem* 46:4265–4272.
24. Scheibel T, Lindquist SL (2001) The role of conformational flexibility in prion propagation and maintenance for Sup35p. *Nat Struct Biol* 8:958–962.
25. Luhrs T, *et al.* (2005) 3D structure of Alzheimer's amyloid-β(1–42) fibrils. *Proc Natl Acad Sci USA* 102:17342–17347.
26. Porat Y, Abramowitz A, Gazit E (2006) Inhibition of amyloid fibril formation by polyphenols: Structural similarity and aromatic interactions as a common inhibition mechanism. *Chem Biol Drug Des* 67:27–37.
27. Makin OS, Atkins E, Sikorski P, Johansson J, Serpell LC (2005) Molecular basis for amyloid fibril formation and stability. *Proc Natl Acad Sci USA* 102:315–320.
28. Esler WP, *et al.* (1996) Point substitution in the central hydrophobic cluster of a human β-amyloid congener disrupts peptide folding and abolishes plaque competence. *Biochemistry* 35:13914–13921.
29. Hilbich C, Kisters-Woike B, Reed J, Masters CL, Beyreuther K (1992) Substitutions of hydrophobic amino acids reduce the amyloidogenicity of Alzheimer's disease β A4 peptides. *J Mol Biol* 228:460–473.
30. Hess S, Lindquist SL, Scheibel T (2007) Alternative assembly pathways of the amyloidogenic yeast prion determinant Sup35-NM. *EMBO Rep* 8:1196–1201.

Supporting Information

Wang *et al*. 10.1073/pnas.0801934105

SI Results

DAPH-1 and DAPH-7 Do Not Affect tau, α-syn, or ure2 Amyloidogenesis. Amyloid fibers are proposed to share generic assembly pathways and final structures (9). Could DAPH-1 or DAPH-7 inhibit the amyloidogenesis of unrelated proteins? We tested the effects of DAPH-1 and DAPH-7 on the amyloidogenesis of tau, which is connected with AD and various tauopathies; α-syn, which is connected with Pakinson's Disease; and Ure2, another yeast prion protein (10, 11). DAPH-1 and DAPH-7 had no effect on tau, α-syn, or Ure2 fiber assembly even at a 4-fold molar excess over the respective protein, as determined by ThT (Fig. S2*A*) and sedimentation analysis (data not shown). Furthermore, DAPH-1 and DAPH-7 did not disassemble tau, α-syn, or Ure2 fibers (Fig. S2*B*). These data demonstrate that DAPHs do not interfere with ThT binding by some nonspecific mechanism. Moreover, they indicate that DAPH-1 and DAPH-7 are not general, nonspecific inhibitors of amyloidogenesis, in contrast to select other small molecules, such as CR or EGCG.

DAPH-1, DAPH-7, and DAPH-12 Do Not Powerfully Remodel Mammalian Prions. Next, we tested DAPH activity against mammalian prions. Although amyloids can be formed from purified prion protein (PrP), they are considerably less infectious than PrP assemblies from infected brains (12). Hence, we treated brain homogenates from mice that were terminally ill from RML prion infection with DAPH-1, DAPH-7, DAPH-12, or DMSO. Treated homogenates were serially diluted and injected intracranially into mice to assess prion titers. Although surrogate markers of infectivity have been developed, this remains the only stringent test for the presence of prions (13). We observed no increase in incubation time (from inoculation until death) between DMSO- and DAPH-treated inoculates (Fig. S2*C*). However, a subset of mice (≈33–50%) inoculated with the most diluted homogenate (1.5 × $\log LD_{50}$) of DAPH-1-, DAPH-7-, or DAPH-12-treated homogenates (but not DMSO controls) survived longer than 336 days and were free of prion disease symptoms (Fig. S2*C*). DAPH-treated RML brain homogenates had no apparent reduction in the amount of PK-resistant prion protein (Fig. S2*D*). Thus, the DAPHs tested may very subtly remodel mammalian prions and slightly reduce their infectivity.

SI Materials and Methods

Small Molecules. DAPH-1, DAPH-7, and DAPH-12 were synthesized as described (1). DAPH-6 and staurosporine aglycone were from Sigma.

Studies with tau, Ure2, and α-synuclein. Recombinant tau (65-kDa human form) was purchased from Sigma. Ure2 and α-syn were purified as described (2, 3). Ure2, tau, and α-syn fibrillization were performed and monitored as described (2–4).

Fiber Assembly and Disassembly Reactions. NM fibrillization was monitored by using either EM, SDS resistance, sedimentation analysis, Congo Red (CR) binding, or Thioflavin T (ThT) fluorescence (5, 6).

CR binding was performed by diluting reactions in assembly buffer (AB) [40 mM Hepes-KOH (pH 7.4), 150 mM KCl, 20 mM $MgCl_2$, and 1 mM DTT] containing CR. This yielded final concentrations of 20 μM CR and 0.5 μM NM. After a 30-min incubation, absorbance was measured at 477 and 540 nm. CR binding was measured as described (5). Similarly for ThT, reactions were diluted 10-fold in AB containing ThT to yield final concentrations of 20 μM ThT and 0.5 μM NM. After a 10-min incubation, reactions were then excited at 450 nm (bandwidth 5 nm), and emission at 482 nm (bandwidth 10 nm) was recorded. Dilution of reactions eliminated any spectroscopic interference by the various DAPHs and also was used for the pyrene and acrylodan fluorescence experiments.

Sedimentation was at 436,000 × *g* for 10min at 25°C. To assess SDS solubility, AB was modified to include 125 mM NaCl and 25 mM KCl to circumvent solubility issues induced by potassium dodecyl sulfate (5, 6). The amount of SDS-soluble (2% SDS, 25°C) NM was determined by quantitative densitometry of Coomassie-stained gels. Values obtained from densitometry were converted to units of pmol by comparison to standard curves with known amounts of SDS-soluble NM. From this value, the amount of SDS-insoluble NM was calculated.

Protein Transformation. Yeast cells from a W303-derived yeast strain (*MATα leu2-3,-112 his3–11 trp1-1 ura3-1 ade1-14 can1-100* [*pin*$^-$] [*psi*$^-$] [*ure-o*]) that contained an *ADE1* mutation suppressible by [*PSI*$^+$] were transformed with NM proteins and a *URA3* plasmid (7, 8). NM from DAPH-treated samples was recovered by ultracentrifugation at 436,000 × *g* for 1 h at 25°C. SDS/PAGE revealed that 90–100% of NM was recovered in this way. Pellet fractions were then washed five times with 500 μl of AB to remove any small molecule, and NM was then resuspended in the transformation mix (7, 8). The proportion of Ura$^+$ transformants that acquired [*PSI*$^+$] was determined (7). Very similar results were obtained by using another yeast strain, 74-D694.

Mammalian Prion Studies. RML strain prion brain homogenates (1%) were incubated for 48 h at room temperature with either DMSO (1%), DAPH-1, DAPH-7, or DAPH-12 (200 μM). Subsequently, 10-fold dilution series were made of these homogenates, and ≈30 μl was injected intracranially into 2.5-month-old female CD1 mice. The survival of these mice was monitored up to 336 days, when we terminated the experiment. Alternatively, homogenates were either left untreated or treated with 50 μg/ml proteinase K (PK) for 1 h. The levels of prion protein were then determined by immunoblot.

1. Hennessy EJ, Buchwald SL (2005) Synthesis of 4,5-dianilinophthalimide and related analogues for potential treatment of Alzheimer's disease via palladium-catalyzed amination. *J Org Chem* 70:7371–7375.
2. Kessler JC, Rochet JC, Lansbury PT, Jr (2003) The N-terminal repeat domain of α-synuclein inhibits β-sheet and amyloid fibril formation. *Biochemistry* 42:672–678.
3. Shorter J, Lindquist S (2006) Destruction or potentiation of different prions catalyzed by similar Hsp104 remodeling activities. *Mol Cell* 23:425–438.
4. Chirita C, Necula M, Kuret J (2004) Ligand-dependent inhibition and reversal of tau filament formation. *Biochemistry* 43:2879–2887.
5. Chernoff YO, Uptain SM, Lindquist SL (2002) Analysis of prion factors in yeast. *Methods Enzymol* 351:499–538.
6. Shorter J, Lindquist S (2004) Hsp104 catalyzes formation and elimination of self-replicating Sup35 prion conformers. *Science* 304:1793–1797.
7. Krishnan R, Lindquist SL (2005) Structural insights into a yeast prion illuminate nucleation and strain diversity. *Nature* 435:765–772.
8. Tanaka M, Chien P, Naber N, Cooke R, Weissman JS (2004) Conformational variations in an infectious protein determine prion strain differences. *Nature* 428:323–328.
9. Nelson R, Eisenberg D (2006) Structural models of amyloid-like fibrils. *Adv Protein Chem* 73:235–282.
10. Shorter J, Lindquist S (2005) Prions as adaptive conduits of memory and inheritance. *Nat Rev Genet* 6:435–450.

11. Skovronsky DM, Lee VM-Y, Trojanowski JQ (2006) Neurodegenerative diseases: New concepts of pathogenesis and their therapeutic implications. *Annu Rev Pathol Mech Dis* 1:151–170.
12. Legname G, *et al*. (2004) Synthetic mammalian prions. *Science* 305:673–676.
13. Prusiner SB (2004) *Prion Biology and Diseases* (Cold Spring Harbor Lab Press, Cold Spring Harbor, NY).
14. Mukhopadhyay S, Krishnan R, Lemke EA, Lindquist S, Deniz AA (2007) A natively unfolded yeast prion monomer adopts an ensemble of collapsed and rapidly fluctuating structures. *Proc Natl Acad Sci USA* 104:2649–2654.

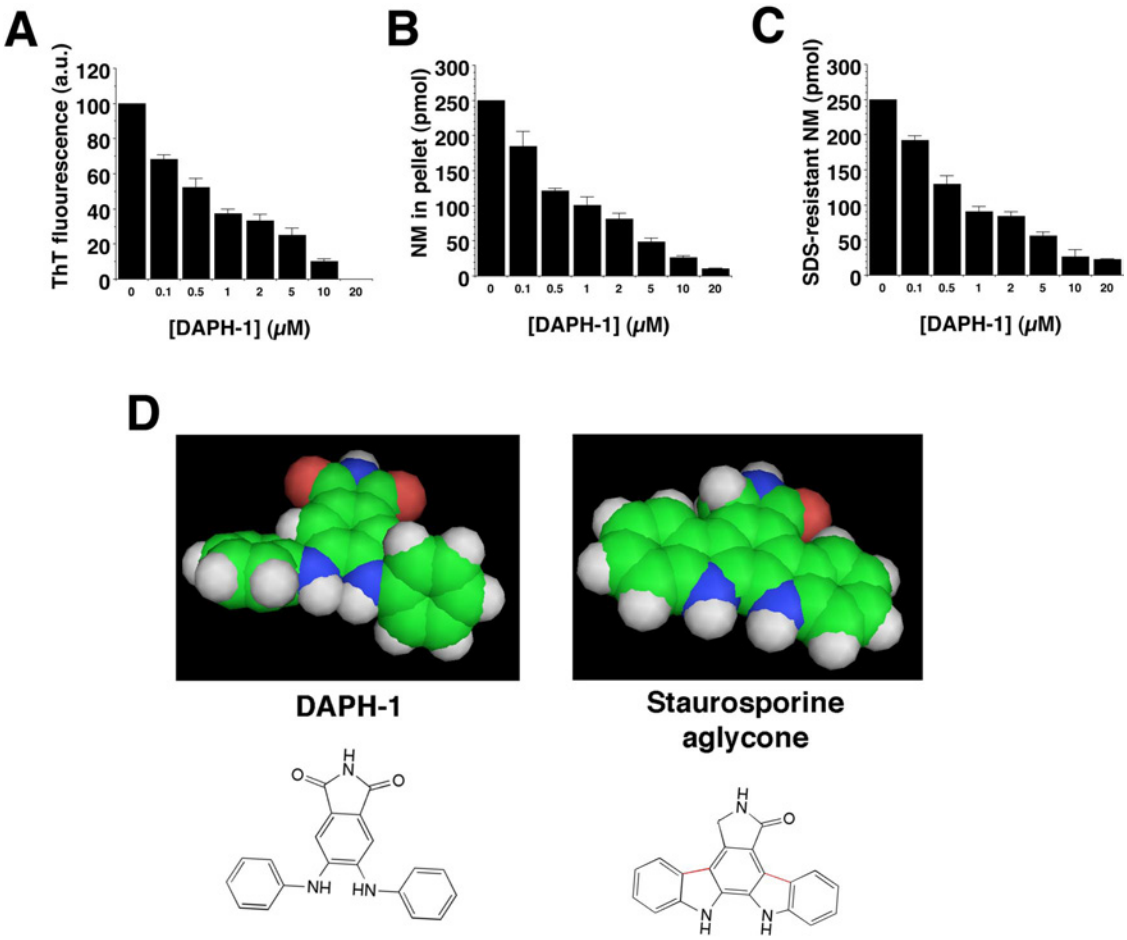

Fig. S1. Inhibition of spontaneous NM fibrillization by DAPHs. (*A–C*) Spontaneous, rotated (80 rpm) NM (5 μM) fibrillization after 4 h in the presence of 0–20 μM DAPH-1. Fibrillization was monitored by ThT fluorescence (*A*), sedimentation analysis (*B*), or SDS resistance (*C*). Values represent means $\pm$ SD ($n = 3$). (*D*) Space filling models of DAPH-1 and SA. Note the propeller-shaped, aplanar conformation of DAPH-1 and the planar conformation of SA. Line drawings of DAPH-1 and SA also are shown.

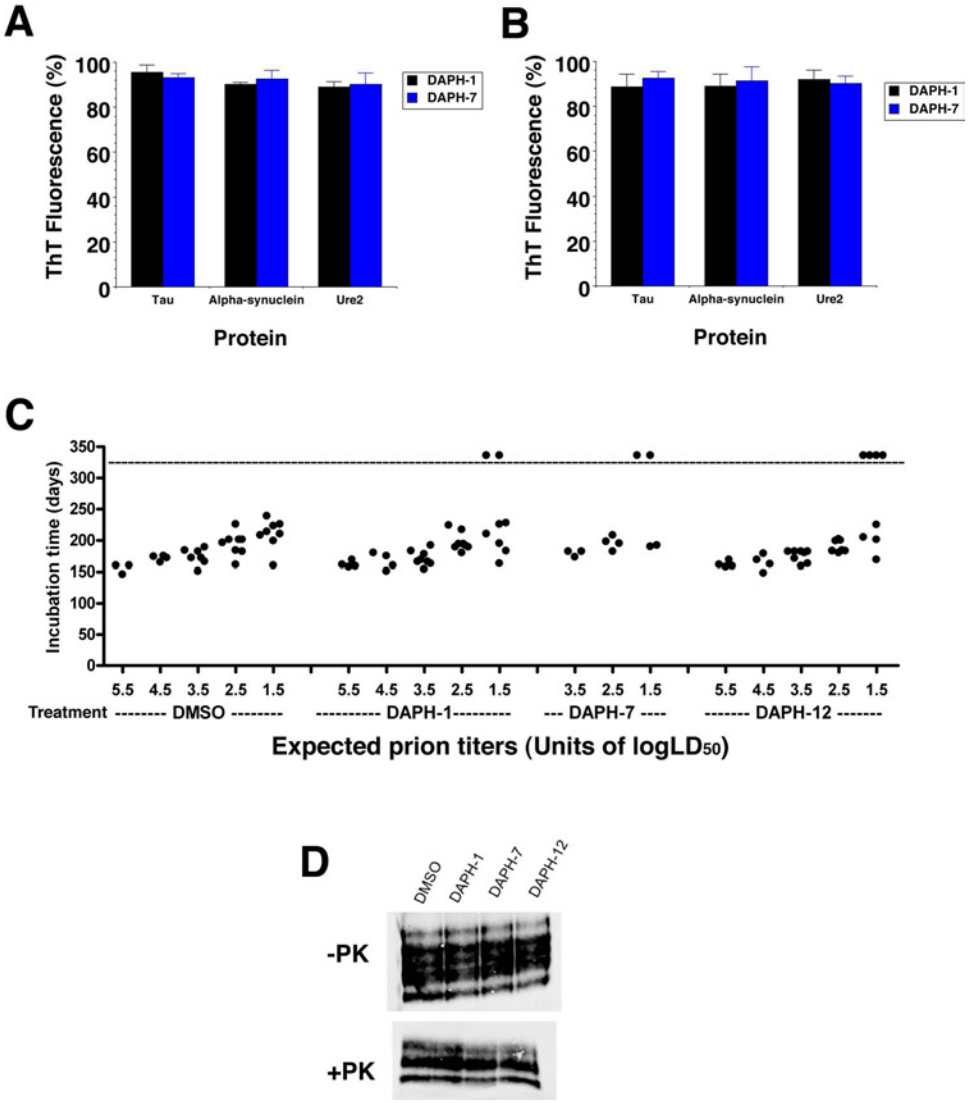

Fig. S2. Effects of DAPHs on tau, α-synuclein, Ure2, and PrP. (*A*) tau (20 μM), α-synuclein (80 μM), or Ure2 (5 μM) were incubated for 24 h in the presence of a 4-fold excess of the indicated DAPH. Fiber assembly was measured by ThT fluorescence; 100% indicates values obtained in the absence of DAPHs. Values represent means $\pm$ SD ($n = 3$). (*B*) Tau, α-synuclein, or Ure2 fibers (10 μM monomer) were incubated with the indicated DAPH (40 μM) for 24 h at 25°C. Fiber integrity was measured by ThT fluorescence; 100% indicates values for untreated fibers. Values represent means $\pm$ SD ($n = 3$). (*C*) RML strain prion brain homogenates (1%) were incubated for 48 h at room temperature with either DMSO (1%), DAPH-1, DAPH-7, or DAPH-12 (200 μM). Subsequently, 10-fold dilution series were made of these homogenates, which were injected intracranially into CD1 mice ($n = 3$–8 per group). Values on the *x* axis correspond to expected prion titers in units of $\log LD_{50}$. The experiment was terminated at 336 days, indicated by a dashed line. Surviving mice were devoid of scrapie symptoms. (*D*) RML strain prion brain homogenates (1%) were incubated for 48 h at room temperature with either DMSO (1%), DAPH-1, DAPH-7, or DAPH-12 (200 μM). Homogenates were then either left untreated or treated with 50 μg/ml PK for 1 h. The levels of prion protein were then determined by immunoblot.

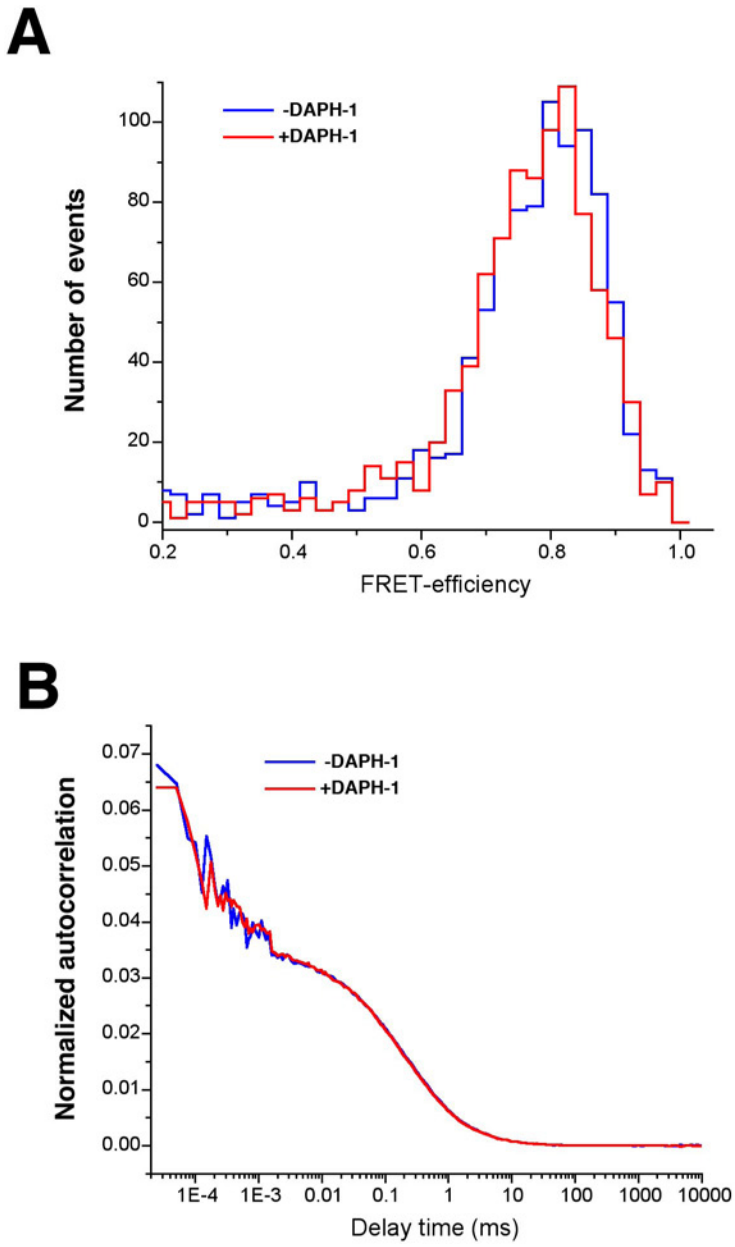

Fig. S3. DAPH-1 does not affect the compression or conformational dynamics of monomeric NM. (*A*) Single-molecule FRET-efficiency distributions for monomeric NM (21C/121C) labeled by using Alexa488 (donor) and Alexa594 (acceptor) in the absence (blue) and presence (red) of DAPH-1, showing NM conformation is unaffected by DAPH-1 in the monomeric form. Zero peaks ($<$0.2E) are not shown because they contain no relevant information (14). Labeled NM and DAPH concentrations were 100 pM and 100 nM, respectively. (*B*) Normalized FCS autocorrelation curves for NM (C38) labeled by using Alexa488 in the absence (blue) and presence (red) of DAPH-1 showing the fast conformational fluctuation and the diffusion components of monomeric NM are unaffected by DAPH-1 (14). Labeled NM and DAPH concentrations were 20 nM and 2 μM, respectively.